Contents lists available at SciOpen

Food Science and Human Wellness

journal homepage: https://www.sciopen.com/journal/2097-0765

Lacticaseibacillus rhamnosus Fmb14 ameliorates hyperuricemia-induced hepatocyte pyroptosis via NLRP3 inflammasome cascade inhibition

Hongyuan Zhao[a], Xiaoyu Chen[a], Li Zhang[b], Fanqiang Meng[a], Libang Zhou[a], Zhaoxin Lu[a,*], Yingjian Lu[c,*]

[a] *College of Food Science & Technology, Nanjing Agricultural University, Nanjing 210095, China*
[b] *Institute of Vegetable, Gansu Academy of Agricultural Sciences, Lanzhou 730070, China*
[c] *College of Food Science & Engineering, Nanjing University of Finance and Economics, Nanjing 210023, China*

ARTICLE INFO

Article history:
Received 1 December 2022
Received in revised form 19 December 2022
Accepted 12 January 2023

Keywords:
Lacticaseibacillus rhamnosus Fmb14
Hyperuricemia
Pyroptosis
NLRP3 pathway

ABSTRACT

Hyperuricemia is a high-risk factor for the development of gout and renal fibrosis, but the adverse effects of hyperuricemia on the liver have been seriously neglected. This research investigated the ameliorating effect of *Lacticaseibacillus rhamnosus* Fmb14 on hyperuricemia induced liver dysfunction both *in vitro* and *in vivo*. Cell free extracts of high dose *L. rhamnosus* Fmb14 treatment reduced the death rate of HepG2 cell lines from 24.1% to 14.9% by inhibiting NLRP3 recruitment, which was mainly activated by reactive oxygen species release and mitochondrial membrane potential disorder. In purine dietary induced hyperuricemia (PDIH) mice model, liver oedema and pyroptosis were ameliorated after *L. rhamnosus* Fmb14 administration through downregulating the expression levels of NLRP3, caspase-1 and gasdermin-D from 1.61 to 0.86, 3.15 to 1.01 and 5.63 to 2.02, respectively. *L. rhamnosus* Fmb14 administration restored mitochondrial inner membrane protein (MPV17) and connexin 43 from 2.83 and 0.73 to 0.80 and 0.98 respectively in PDIH mice, indicating that dysbiosis of mitochondrial membrane potential was restored in liver. Intriguingly, PDIH pyroptosis stimulates the process of apoptosis, which leads to severe leakage of hepatocytes, and both of pyroptosis and apoptosis were decreased after *L. rhamnosus* Fmb14 treatment. Therefore, *L. rhamnosus* Fmb14 is a promising biological resource to maintain homeostasis of the liver in hyperuricemia and the prevention of subsequent complications.

1. Introduction

Hyperuricemia is a metabolic syndrome defined as an elevation of blood urate concentration beyond solubility[1-2]. In addition a 10% incidence of gout development, recent studies have shown that hyperuricemia is associated with a high risk of developing a variety of other syndromes, including hypertension, acute and chronic kidney disease, obesity, metabolic syndrome, fatty liver and diabetes mellitus[3-4], therefore, the asymptomatic condition of hyperuricemia has been seriously neglected[5]. Hyperuricemia occurs due to both dietary and genetic factors, but the prevalence has increased for modern dietary habitats worldwide. Previous studies have confirmed that monosodium urate (MSU) crystals lead to inflammation[6] or oxidative stress[7-8], but recent studies have strongly indicated that asymptomatic hyperuricemia may induce oxidative stress, proinflammatory signalling and autophagy[1].

Purine is mainly metabolized to uric acid (UA) by xanthine oxidase in the liver, but research on hyperuricemia prevention or treatment has focused on the gut[9] or kidney[10] due to their UA excretion ability. As the major UA metabolism organ, dysfunction or damage to the liver in hyperuricemia[11] needs more attention. NOD-, LRR- and pyrin domain-containing 3 (NLRP3) inflammasome activation leads to caspase-1-mediated proteolytic activation of the interleukin-1β (IL-1β) family of cytokines, which is the target in many inflammatory

* Corresponding authors.
E-mail address: fmb@njau.edu.cn (Z.X. Lu); yingjianlu@nufe.edu.cn (Y.J. Lu)
Peer review under responsibility of Tsinghua University Press.

Publishing services by Tsinghua University Press

http://doi.org/10.26599/FSHW.2022.9250181

diseases[12], and hyperuricemia is one of the participants[13]. In addition to NLRP3 activation, UA has also been reported to stimulate the nuclear transcription factor κB (NF-κB)[14] and p53[15] pathways as a pathogenesis mechanism.

Probiotics have been recognized as key health promoters, and their beneficial effects on metabolism regulation[16], gut barrier enhancement, gut microbiota modulation[17] and inflammation attenuation[18] in the host have been strongly proven. Danger-associated molecular patterns (DAMPs) and pathogen-associated molecular patterns (PAMPs) are two triggers of NLRP3 inflammasome recruitment[19] and *Lactobacillus* has been reported to play an essential role in the inhibition of PAMP-related NLRP3 cascade reactions. Traditional clinical treatment of NLRP3-related diseases targets the inhibition of IL-1β, which is one of the products of the NLRP3 inflammatory pathways[20], but the therapeutic pertinence is low for the universality of IL-1β. *Lactobacillus johnsonii* and *Lactobacillus reuteri* have been reported to inhibit NLRP3 inflammasome activation induced by *Escherichia coli* and C*ampylobacter jejuni*, respectively[21-22].

The adverse impact of UA on hepatocytes may be greatly miscalculated, and *L. rhamnosus* Fmb14 may protect the liver in hyperuricemia. Our previous studies have proven the superiority of *L. rhamnosus* Fmb14 for hyperuricemia amelioration[23]. *L. rhamnosus* Fmb14 could degrade 36.3% inosine and produce intracellular folic acid and riboflavin *in vitro*[24], and decrease 36.8% serum UA through modulation of UA metabolism and transportation, epithelial barrier enhancement and gut microbiota regulation[23]. The protective effect of *L. rhamnosus* Fmb14 on hepatic disease induced by hyperuricemia was evaluated both *in vivo* and *in vitro*. High concentrations of UA were used to stimulate HepG2 cells *in vitro*, and a purine diet-induced hyperuricemia mouse model was used to examine the underlying mechanisms of *L. rhamnosus* Fmb14 on liver protective effects under high UA conditions. In view of the potential important role of *L. rhamnosus* Fmb14 in ameliorating liver failure, we explored the regulatory effect of *L. rhamnosus* Fmb14 on the programmed cell death of hepatocytes.

2. Materials and methods

2.1 Materials and reagents

L. rhamnosus Fmb14 (NCBI accession number: CP101845) was provided by Enzyme Engineering Laboratory, Nanjing Agricultural University (China). Dulbecco's Modified Eagle's medium (DMEM) and fetal bovine serum (FBS) were purchased from Gibco Co., Ltd. (Carlsbad, USA). The UA was purchased from Aladdin Co., Ltd. (Shanghai, China). The primary antibodies against glyceraldehyde-3-phosphate dehydrogenase (GAPDH), NLRP3, gasdermin-D (GSDMD), caspase-1, IL-1β, IL-18, toll-like receptor 4 (TLR4), apoptosis-associated speck-like protein containing CARD (ASC), connexin 43, mitochondrial inner membrane protein (MPV17), acyl-CoA oxidase (Acox), B-cell lymphoma-2 (Bcl2), BCL-2-associated X (Bax), caspase-3, NF-κB, p53, adenosine 5′-monophosphate-activated protein kinase (AMPK) and c-Jun N-terminal kinase (JNK) were purchased from Beyotime Biological Technology Co., Ltd. (Wuhan, China). The secondary antibody goat anti-rabbit IgG (peroxidase conjugate) were obtained from Boster Biological Technology Co., Ltd. (Wuhan, China). The enzyme linked immunosorbent assay (ELISA) kits for IL-1β and IL-18 were purchased from MEIMIAN Institute of Biotechnology Co., Ltd. (Taizhou, China). TUNEL Apoptosis Assay Kit was purchased from Solarbio Science & Technology Co., Ltd. (Beijing, China).

2.2 Preparation of different cell-free extracts (CFEs)

L. rhamnosus Fmb14 was incubated in de Man, Rogosa and Sharpe (MRS) broth culture for 24 h. Then, *L. rhamnosus* Fmb14 was adjust to the concentrations of 10^9 and 10^7 CFU/mL and then centrifuged at 8 000 × *g* for 10 min to collect live microorganisms. Then microorganisms were washed with phosphate buffered saline (PBS) (pH 7.2) three times and finally re-suspend the cell pellets in different suspension solutions. Afterwards, cell suspension was placed in ice bath and treated with ultrasonic disruption for 20 min to break bacterial cells to obtain CFE. After centrifugation (8 000 × *g*) at 4 °C for 10 min, the resulting supernatant was collected for further experiments. The CFE-H and CFE-L were extracts from *L. rhamnosus* Fmb14 at 10^9 and 10^7 CFU/mL, respectively.

2.3 Investigation of apoptosis in HepG2 cells

2.3.1 Morphological observation of apoptosis in HepG2 cells

HepG2 cells were equally seeded in 6-well plates, the effect of different concentrations of UA, CFE-H, CFE-L were tested. Then free medium with PBS treated was set as control, 500 μmol/L UA was set as model, CFE-H and CFE-L treated were added as therapeutic respectively. After 24 h of treatment, the morphology of HepG2 cells was observed under an Eclipse E 100 inverted phase contrast microscope (Nikon, Mississauga, ON, Canada) and were captured at 400 × magnification using infinity digital microscopy camera (Lumenera Co., Ottawa, ON, Canada).

2.3.2 Apoptosis test by labelling (TUNEL) staining in HepG2 cells

The number of apoptotic cells was evaluated by flow cytometry using an FITC-Annexin V Apoptosis Detection kit (BD Biosciences) according to the manufacturer's instructions. In brief, HepG2 cells were seeded in 6-well plates at 2×10^5 cells/well and treated with 500 μmol/L UA and different concentrations of CFE (50 and 100 μL) for 24 h. Cells were washed twice with PBS and re-suspended in 200 μL binding buffer. After addition of 5 μL Annexin V conjugate and incubation for 10 min, the samples were resuspended in 200 μL binding buffer and 5 μL propidium iodide (PI). The cells were examined using the flow cytometer with 10 000 events collected for each sample.

2.4 Measurement of reactive oxygen species (ROS)

The ROS assay was performed as previously described[25]. HepG2 cells were seeded in DMEM supplemented with 10% (*V/V*) of FBS, streptomycin (100 μg/mL), and penicillin (100 units/mL), as well the culture condition was 5% CO_2 and 95% air at 37 °C for 24 h. Then HepG2 cells were plated into 6-well plates at 10^5 cells/well, and incubated with DMEM culture (containing FBS) with 500 μmol/L

UA, and different CFEs (100 μL as CFE-H and 50 μL as CFE-L) of *L. rhamnosus* Fmb14 were added into culture and saline was added as control. Then cell was cultured for 24 h and then the medium was discarded and the cells were collected after 2 min pancreatin treated, and then stained with 10 μmol/L DCFH-DA (Cellular ROS Assay Kit, S0033S, Beyotime Biotech, Shanghai, China) fluorescent probe at 37 °C for 30 min and washed 3 times with cold PBS. The level of ROS was determined flow cytometry and all groups were repeated 3 times.

2.5 Measurement of mitochondrial membrane potential (MMP)

HepG2 cells were cultured in DMEM supplemented with 10% (*V*/*V*) of FBS, streptomycin (100 μg/mL), and penicillin (100 units/mL), as well the culture condition was 5% CO_2 and 95% air at 37 °C. Then HepG2 cells were plated into 6-well plates at 10^5 cells/well, and incubated with DMEM culture (containing FBS) with 500 μmol/L UA, and CFE-L for 24 h. The MMP assay kit with JC-1 was used to measure the change of MMP according to the manufacturer's instructions. The stained cells were analyzed using fluorescence microscope.

2.6 RNA extraction and quantitative polymerase chain reaction (qPCR)

The culture of HepG2 and the treated were described as in section 2.5. Total RNA were isolated from cultured HepG2 cells by homogenization in TRIzol reagent (TransGen Biotech., Beijing, China), used for RNA extraction. Then, RNA was reverse-transcribed into cDNA using a HiScript II Q RT SuperMix kit (Vazyme Biotech Co., Ltd., Nanjing, China) and the quality of cDNA was measured using a NanoDrop 2000 Spectrophotometer (Thermo Fisher Scientific Inc., Waltham, USA). qPCR was operated with 2 × Hieff™ SYBR Green Master Mix (Yeasen Biotech Co., Ltd., Shanghai, China) and a real-time PCR (RT-PCR) detection (Applied Biosystem, Carlsbad, USA) at the following cycling conditions: 95 °C for 2 min, followed by 40 cycles of 95 °C for 5 s, 60 °C for 30 s and 72 °C for 30 s. The melting curve was also done from 65 to 95 °C with 0.5 °C/s increments to exclude unspecific amplification after the last reaction. The relative expression levels in terms of fold changes of target genes were calculated by $2^{-\Delta\Delta Ct}$ method. The primers were shown in Table S1. The melting curve was used to check the specificity of the primers.

2.7 Determination of cytokines

The culture of HepG2 and the treated were described as in section 2.4. The intracellular and secreted IL-1β and IL-18 of HepG2 were measured by ELISA kit (MEIMIAN Technology, Taizhou, China) according to manufactures' protocols. The absorbance was detected using a microplate reader at 450 nm. The secreted IL-1β and IL-18 tested in the medium of the cell and 100 μL RIPA was added to every plate to lyse cells and intracellular proteins were harvest from supernatant after centrifugation at 4 000 × *g*.

2.8 Determination of caspase-1 and NLRP3 by immunocytochemistry (ICC)

Pre-set a 50 mm × 50 mm coverslip in every well in the 6-well plates and the cell were then cultured in the plates for 24 h at 37 °C. The groups were divided as described in section 2.5 and cell on the coverslip was fixed in the 4% paraformaldehyde for 10 min. Cells were treated in 3% H_2O_2 for 10 min to scavenging peroxide and blocked non-specific site by normal goat serum for 1 h at 37 °C in dark. Slides were incubated with primary antibody overnight at 4 °C. This was then detected by incubation with horseradish peroxidase-tagged antibody followed by color development using 3,3'-diaminobenzidine tetrahydrochloride (DAB) as chromogen. Stained slides were photographed in ECLIPSE 80i bright-field microscope (Nikon Co., Tokyo, Japan) and evaluated by mean optical density (MOD) by ImageJ as ICC scores.

2.9 Investigation of liver apoptosis in purine induced hyperuricemia mice

The mice livers were obtained from the purine dietary induced hyperuricemia (PDIH) mice described by Zhao et al.[23]. Specifically, the animal experiments were carried out according to regulations controlled by Laboratory Animal's Research Centre of Nanjing Agricultural University (Nanjing, China). All experimental protocols were approved by Ethics Committee of Nanjing Agriculture University (Nanjing, China, Approval number: NJAU No. 20210311012). Four-week old specific pathogen-free (SPF) class of male Kunming mice was purchased from Yangzhou University (Jiangsu, China) and all animals were kept under SPF conditions. Thirty mice were distributed into 3 groups of 10 mice in each group and the model were established by 12 weeks orally administrated inosine (0.25 mg/100 g body weight per day) and potassium oxonate (0.35 mg/100 g body weight per day). The Fmb14-treated group was administrated 100 μL *L. rhamnosus* Fmb14 dissolved in saline with concentrations at 10^9 CFU/mL while control group administrated same volume of saline. The serum UA levels of the control, model and Fmb14-treated groups reached 98.7, 179.1 and 113.2 μmol/L, respectively.

2.10 Histological analysis

The liver samples were rinsed with PBS, after which the intestinal and colons was taken with a length of 1 cm, while whole kidneys were employed. The samples were immersion in a 4% paraformaldehyde solution at room temperature for more than 1 day. Later, the samples were sent to the Hycell Biotechnology (Nanjing, China) and staining with hematoxylin and eosin (HE) and TUNEL kit. The morphology of the sections in different groups were observed under a ECLIPSE 80i microscope (Nikon Co., Japan).

2.11 Determination of pyroptosis and apoptosis related gene expression by RT-qPCR

Total RNA was extracted from mouse intestinal organoids or tissues by RNAiso Plus (Takara, Japan). RNA was reverse transcribed with a PrimeScript RT Reagent Kit (Takara) and customized primers

designed to amplify fragments of the target genes with SYBR master mix (Takara) using the QuantStudio 7 Flex System (Applied Biosystems, USA). Relative amounts of mRNA were calculated using the $2^{-\Delta\Delta Ct}$ method, and *GAPDH* served as the housekeeping gene. Fold change values were calculated for genes expressed in experimental vs. control conditions. The primers used in this study are listed in Table S2.

2.12 Western blot analysis of the liver

Fresh liver was ground using a handheld grinder (Jingxin, Shanghai, China) on ice, after which the suspension of samples was obtained at low speed centrifugation (8 000 r/min, 10 min).

The liver tissues (500 mg) were placed in a mortar and together with liquid nitrogen and promptly crushed into powder. The powder was added to 500 μL RIPA lysis buffer (10 μL/mg) (Beyotime Biotech, Shanghai, China) which containing phenylmethylsulfonyl fluoride (PMSF), and lysed on ice for 30 min after vortex. Protein samples were extracted from the supernatant after the mixture was centrifuged at 12 000 × *g* for 5 min at 4 °C. The protein samples were separated on a 12% sodium dodecyl sulfate polyacrylamide gel electropheresis (SDS-PAGE) and transferred to nitrocellulose (NC) membranes, which were blocked in Tris-buffered saline and 0.1% Tween-20 (TBST) with 5% nonfat dry milk and treated overnight at 4 °C with primary antibodies. The membranes were then incubated for 2 h at room temperature with HRP-conjugated goat anti-rabbit IgG secondary antibodies (Beyotime Biotech, Shanghai, China) and exposed to MiniChem610 (SageCreation, Beijing, China). The protein bands were quantified using ImageJ software..

2.13 Statistical analysis

Statistical analysis and Spearman correlation analysis were performed using SPSS v.17.0 software. $P < 0.05$ indicated statistical significance. Data were analyzed using one-way analysis of variance (ANOVA). The significant differences between the two groups were analyzed using independent samples *t*-test.

3. Results

3.1 L. rhamnosus Fmb14 reduces death rate of UA-induced HepG2 cell lines

To evaluate the effect of *L. rhamnosus* Fmb14 on UA-induced death of HepG2 cell lines, morphological images were observed. The number of HepG2 cells with abnormal morphology increased with increasing UA from 52.8 to 183.0 for 24 h, and the number of cells with abnormal morphology was not changed by CFE-H and CFE-L from *L. rhamnosus* Fmb14 (Fig. 1A). Then, UA and CFEs of *L. rhamnosus* Fmb14 were both added, and the ameliorating effect of CFEs on UA-induced death was observed (Fig. 1A). The angiogenesis ability of CFE-H on UA-induced death of HepG2 cells was further confirmed by the assessment of FITC/PI fluorescence intensity (Fig. 1B). The results showed that CFE-H reduced the toxicity induced by UA, as the rate of abnormal was reduced from 24.1% to 14.9% (Fig. 1B). The viable and nonviable apoptotic cells treated with CFE-H were significantly restored compared to those in the model group (Fig. 1C) ($P < 0.05$).

3.2 L. rhamnosus Fmb14 decreases ROS and restores MMP in UA-induced HepG2 cell lines

Disorders of HepG2 cell lines are often related to oxidative stress and inflammation. Elevated intracellular ROS levels were observed in HepG2 cells lines when stimulated with 500 μmol/L

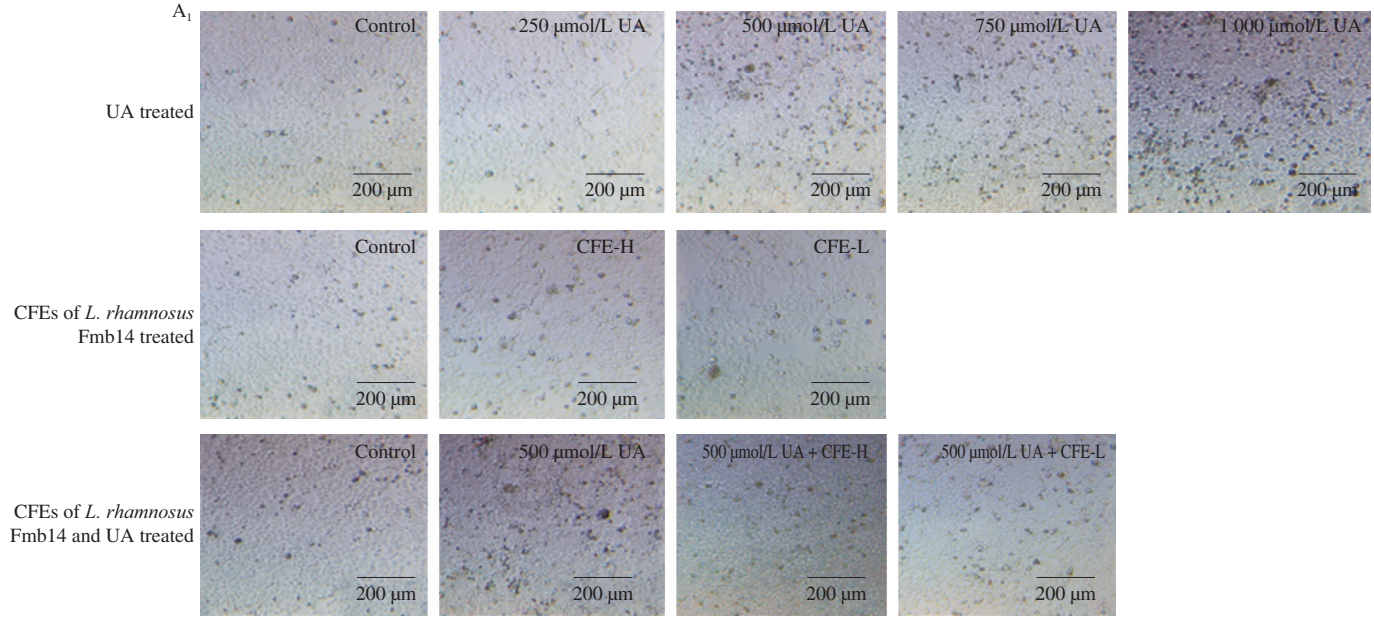

Fig. 1 Effects of CFE of *L. rhamnosus* Fmb14 on the reduction of cell pyroptosis in HepG2 cells under high-UA conditions. (A) Effect of UA and CFE of *L. rhamnosus* Fmb14 on cell morphology in HegG2 cells for 24 h. (B−C) Flow cytometric analysis of apoptotic status in HepG2 cells. (B_1) Control; (B_2) Model; (B_3) CFE-H; (B_4) CFE-L. (C) Percentage of viable apoptotic cell, non-viable apoptotic cell, and non-viable non-apoptotic cell. Areas represent cells in different stages of apoptosis. The mean ± standard deviation (SD) are shown by bars ($n > 3$ per group), and different lowercase letters represent significant differences at $P < 0.05$. The same below.

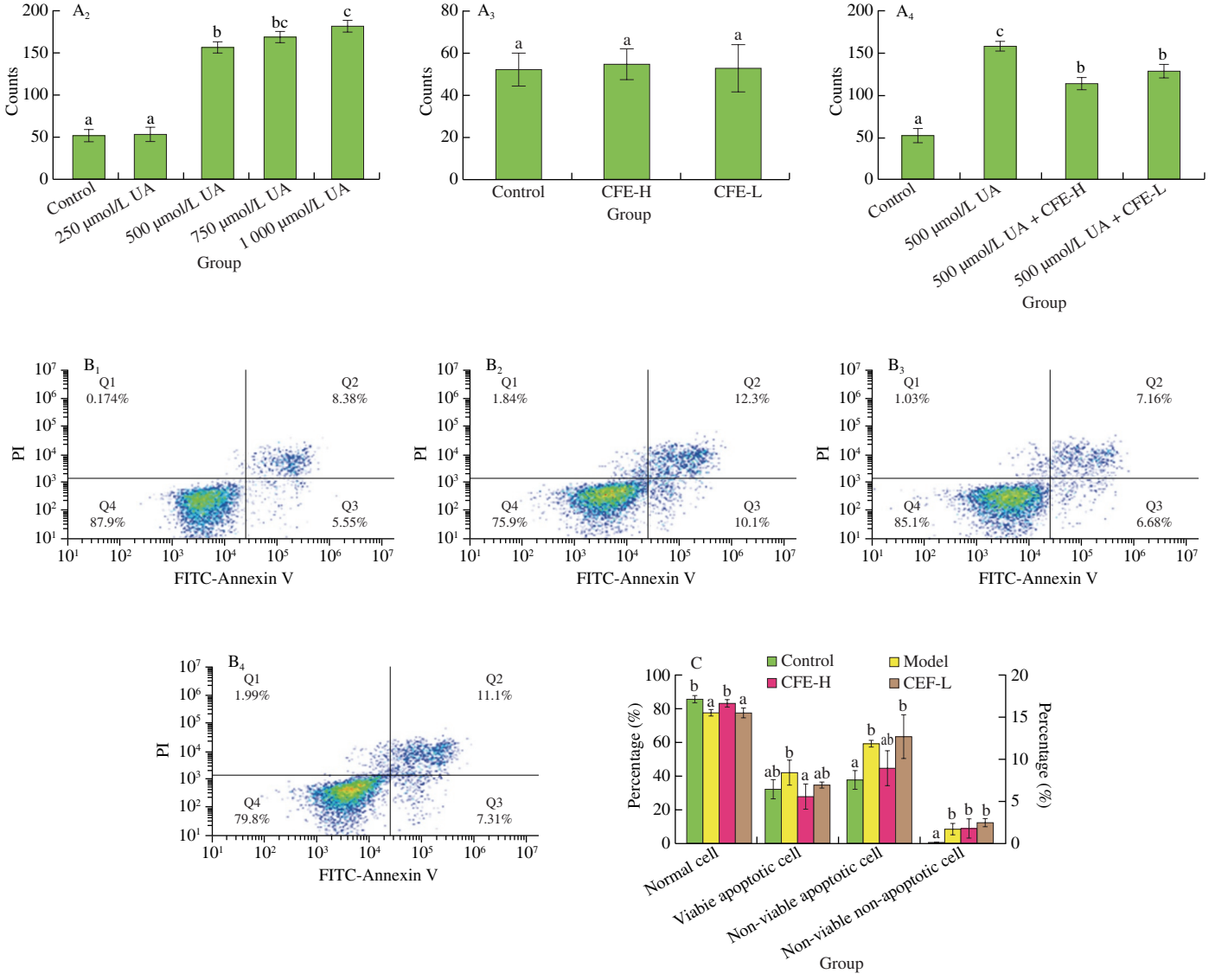

Fig. 1 (*Continued*)

UA (Fig. 2A). Then, CFE-H of *L. rhamnosus* Fmb14 was added to a culture containing 500 μmol/L UA, and the results showed that ROS production was notably increased from 17.9% to 22.9% in the UA model group compared to the control group at 24 h ($P < 0.05$). Then, CFE-H treatment effectively reduced intracellular ROS to 14.5% in the UA model ($P < 0.05$) for 24 h (Fig. 2A). The increase in ROS was accompanied by abnormalities in MMP, so a JC-1 probe was used to determine the change in MMP, and the results showed the same tendency of MMP to ROS (Fig. 2B).

3.3 L. rhamnosus Fmb14 downregulates the gene expression of NLRP3 pathway components in UA-induced HepG2 cell lines

The gene expression levels of *IL-1β*, *IL-6*, *IL-18*, *NF-κB*, *Nrf-2*, and *Tlr-4*, which are biomarkers of different types of inflammatory pathways, *Bcl*, *Bax*, *caspase-1*, *caspase-3*, and *Nlrp3*, which are biomarkers of apoptosis and proptosis, *SOD, CAT, iNOS* and *GSH-Px*, which are biomarkers of oxidative stress, and *CXCL-1*, *CXCL-2*, *CCL-20*, and *CCL-2*, which are biomarkers of the immune system, were all measured by qPCR. UA stimulated the activation of oxidative stress- and inflammation-related gene expression, and some of them could be recovered by CFE-H of *L. rhamnosus* Fmb14 (Fig. 3A). The effects of CFE-H on UA-stimulated HepG2 cells on the expression levels of *Nlrp3* (from 1.45 to 0.94), *IL-1β* (from 1.44 to 1.11), and *IL-18* (from 1.47 to 1.20) indicated that UA led to pyroptosis and *L. rhamnosus* Fmb14 could mainly regulate the dysbiosis.

The *in vitro* addition of 500 μmol/L UA to the culture medium induced higher levels of secreted IL-1β and IL-18 than the control group, and CFE-H treatment significantly decreased the levels of the two ILs (Figs. 3B and C). The levels of intracellular IL-1β and IL-18 were not changed by UA stimulation (Fig. S1). Subsequently, the effects of UA and CFE-H treatment on NLRP3 were further determined by ICC. The results indicated that CFE-H of *L. rhamnosus* Fmb14 decreased NLRP3 and caspase-1 expression induced by UA (Figs. 3D and E).

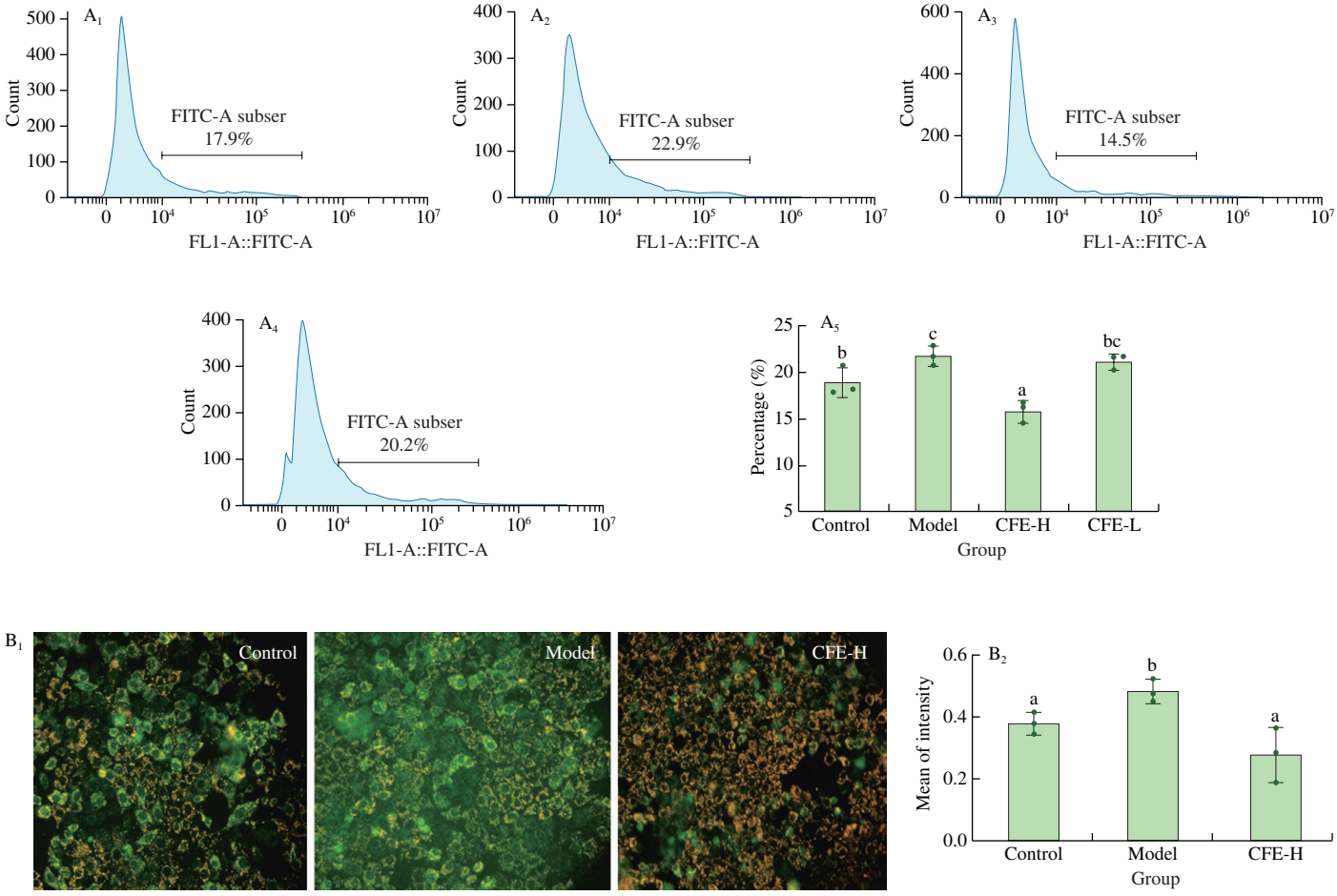

Fig. 2 Effects of CFE on UA-induced pyroptosis of ROS and MMP in HepG2 cells. (A) Flow cytometric dot plots and quantification of flow cytometry-provided ROS counts. (A_1) Control; (A_2) Model; (A_3) CFE-H; (A_4) CFE-L; (A_5) ROS level. The gate indicates that the fluorescence intensity is greater than 10^4. (B_1) Morphological images of cells under a fluorescence microscope with a magnification of 100 μm. Normal mitochondria present a red colour, while mitochondria with reduced membrane potential present a green colour. (B_2) Mitochondrial membrane potential.

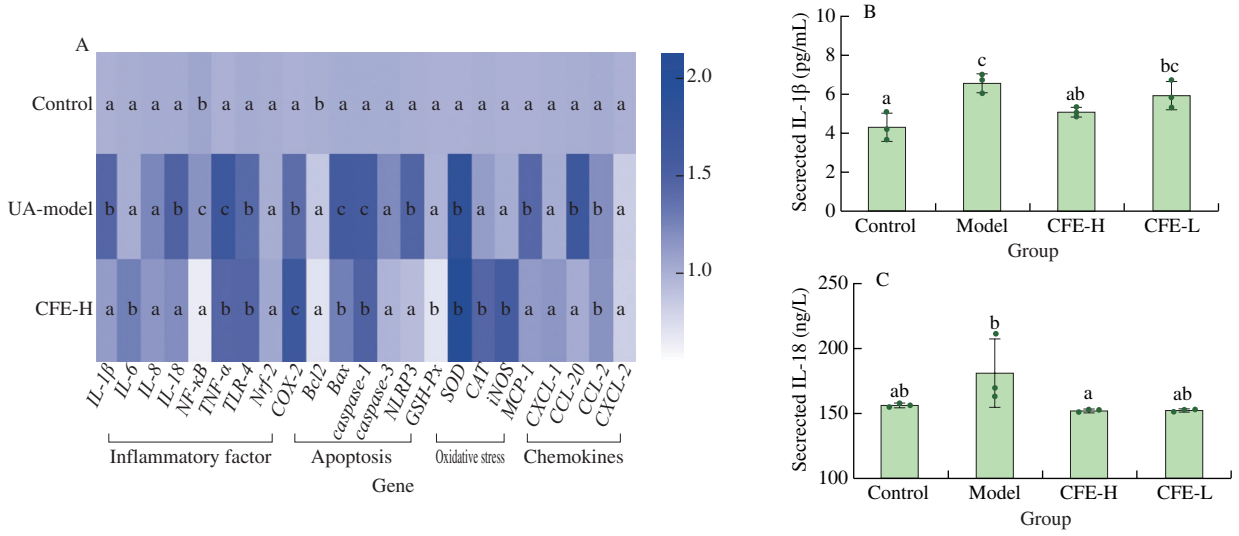

Fig. 3 Target biomarkers of *L. rhamnosus* Fmb14 on the amelioration of pyroptosis induced by UA. (A) Heatmap of the ameliorating effect of *L. rhamnosus* Fmb14 CFE-H on UA stimuli at the mRNA level in HepG2 cells. (B-C) The effect of *L. rhamnosus* Fmb14 CFE on UA stimulation of secreted cytokines. Immunocytochemistry images of (D) caspase-1 and (E) NLRP3.

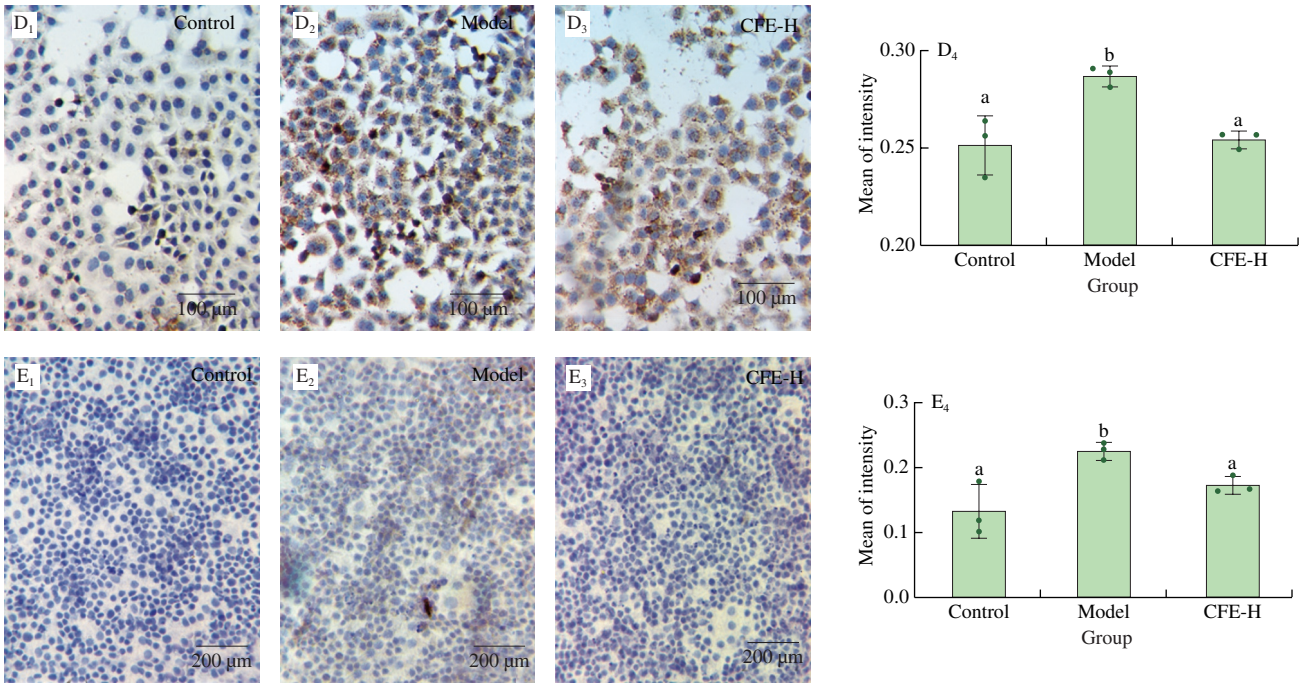

Fig. 3 (*Continued*)

3.4 L. rhamnosus Fmb14 decreased liver pyroptosis in purine diet-induced hyperuricemia in mice

After confirming the NLRP3 inhibitory effect of *L. rhamnosus* Fmb14 on UA-induced pyroptosis *in vitro*, the mechanisms by which *L. rhamnosus* Fmb14 inhibits the NLRP3 inflammasome in the liver were investigated *in vivo*. A high purine diet-induced hyperuricemia model was established, and the livers in hyperuricemia mice were tested as shown in Fig. 4. Hepatic injury was evaluated with HE staining under a microscope (Fig. 4A). More sinus congestion and spot-like necrosis in the hepatic lobule were observed in the model groups, and *L. rhamnosus* Fmb14 treatment significantly decreased hepatic injury (Fig. 4A). To confirm the degree of pyroptosis and the protective effect of *L. rhamnosus* Fmb14 on hyperuricemia-induced hepatic injury, TUNEL staining was used to detect liver apoptosis in mice. The results revealed that *L. rhamnosus* Fmb14 administration significantly reduced the hepatocyte death rate (Fig. 4B).

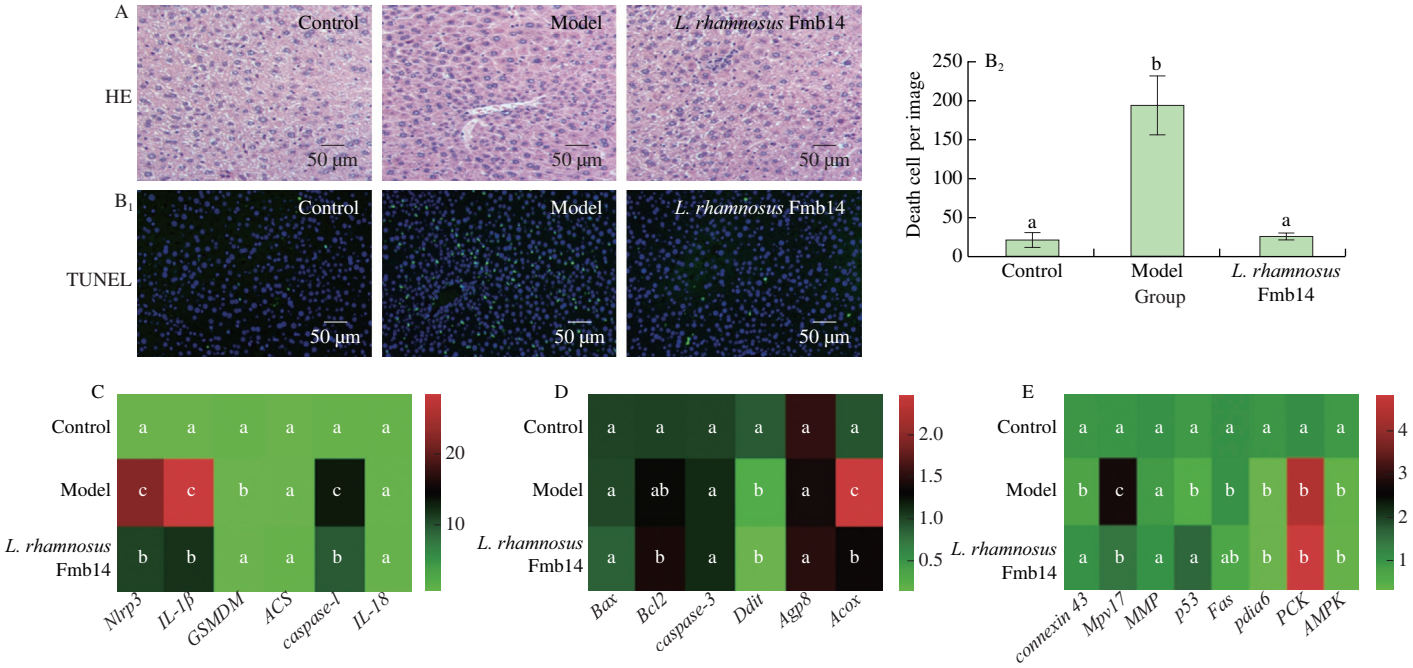

Fig. 4 Amelioration effect of *L. rhamnosus* Fmb14 on liver damage and related biomarkers at the mRNA level in purine-induced hyperuricaemic mice. (A) HE-stained images of the liver. (B) Immunocytochemistry images by TUNEL staining and number of death cell per image of the liver. Heatmaps of (C) pyroptosis, (D) apoptosis and (E) tumour related biomarkers modulated by *L. rhamnosus* Fmb14 administration at the mRNA level.

Then, the mRNA levels of pyroptosis-related (*Nlrp3*, *GSDMD*, *ACS*, *IL-1β* and *IL-18*), apoptosis-related (*Bax*, *Bcl2*, *caspase-3*, *Fas*, *Ddit*, *Agp8* and *Acox*), mitochondria membrane-related and cancer process-related markers in the livers of mice of all 3 groups were measured. The results indicated that the relative mRNA expression levels of markers of pyroptosis were upregulated over 20-fold in the model group compared with the control group and that *L. rhamnosus* Fmb14 administration significantly reduced these alterations (Fig. 4C). In addition to pyroptosis, *L. rhamnosus* Fmb14 also regulates the mRNA expression levels of *Acox*, *connexin 43*, *Mpv17*, *p53 and Fas*, which revealed that *L. rhamnosus* Fmb14 attenuates mitochondrial membrane dysfunction and inhibits the pathological process of the liver (Figs. 4D and E).

3.5 *L. rhamnosus Fmb14 pretreatment suppresses pyroptosis in PDIH mice through NLRP3 inhibition*

The expression levels of NLRP3-related proteins, including NLRP3, caspase-1, GSDMD, ASC, IL-1β and IL-18, were found to be significantly increased in the model group, and *L. rhamnosus* Fmb14 administration downregulated the proteins in the cascade to the levels of the control (Fig. 5A). Specifically, GSDMD, IL-1β, caspase-1 may play the most critical roles in hyperuricemia-induced pyroptosis because the expression levels of these three proteins in the model group were 6.24-, 3.58- and 3.14-fold higher than those in the control group. The expression levels of the whole NLRP3 cascade were decreased in hyperuricemia after *L. rhamnosus* Fmb14 administration for 12 weeks, as NLRP3, caspase-1, ASC, IL-1β, pro-IL-1β and IL-18 were decreased from 1.61-, 3.14-, 1.57-, 3.58-, 1.90- and 3.23-fold to 0.86-, 1.01-, 0.77-, 1.34-, 0.72- and 1.69-fold respectively, compared to the control group (Figs. 5B-I).

Consistent with the *in vivo* results, the causal relationship between purine-induced hyperuricemia and mitochondrial membrane damage in the liver has been clearly confirmed. The expression of MPV17 in the liver was increased to 2.83-fold that of the control group and was restored to 80% that of the control after *L. rhamnosus* Fmb14 treatment (Figs. 6A and C). The expression of connexin 43 was decreased to 73% that of the control group, which led to vacuolization of the liver (Fig. 6B). Apoptosis-related proteins, including Bcl2, Bax, caspase-3 and Acox, were also investigated. Expression of the apoptosis inhibitor Bcl2 (19% of control) was reduced in the hyperuricemia group and was

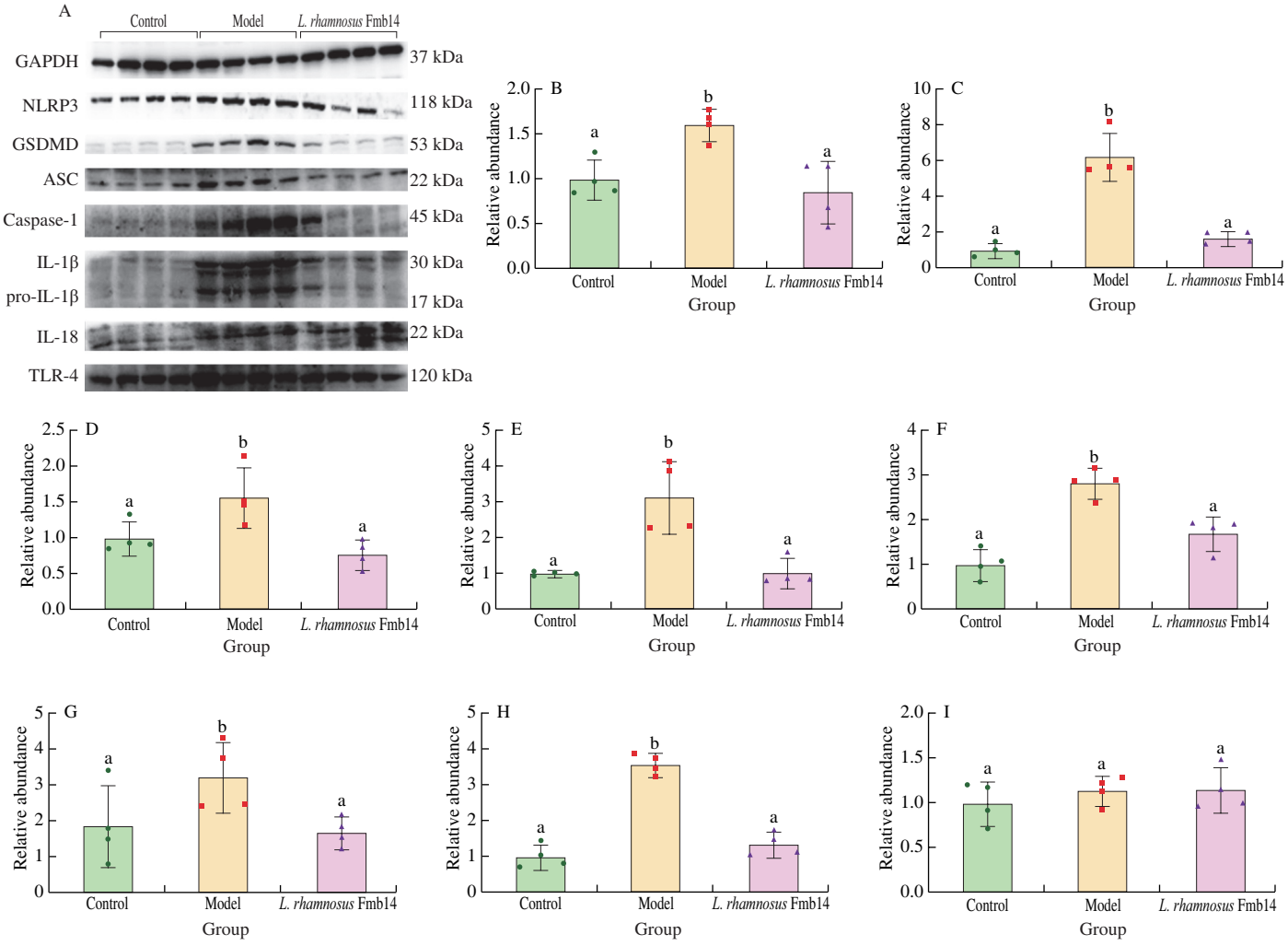

Fig. 5 *L. rhamnosus* Fmb14 administration improves hyperuricemia-induced pyroptosis. (A) Western blot measurement of liver lysates from purine-induced hyperuricaemic mice without and with *L. rhamnosus* Fmb14 administration, including GAPDH, NLRP3, GSDMD, ASC, caspase-1, IL-1β, IL-18 and TLR4. Hepatic protein expression levels of (B) NLRP3, (C) GSDMD, (D) ASC, (E) caspase-1, (F) IL-1β, (G) IL-18, (H) pro-IL-1β, and (I) TLR4. GAPDH was tested as a reference.

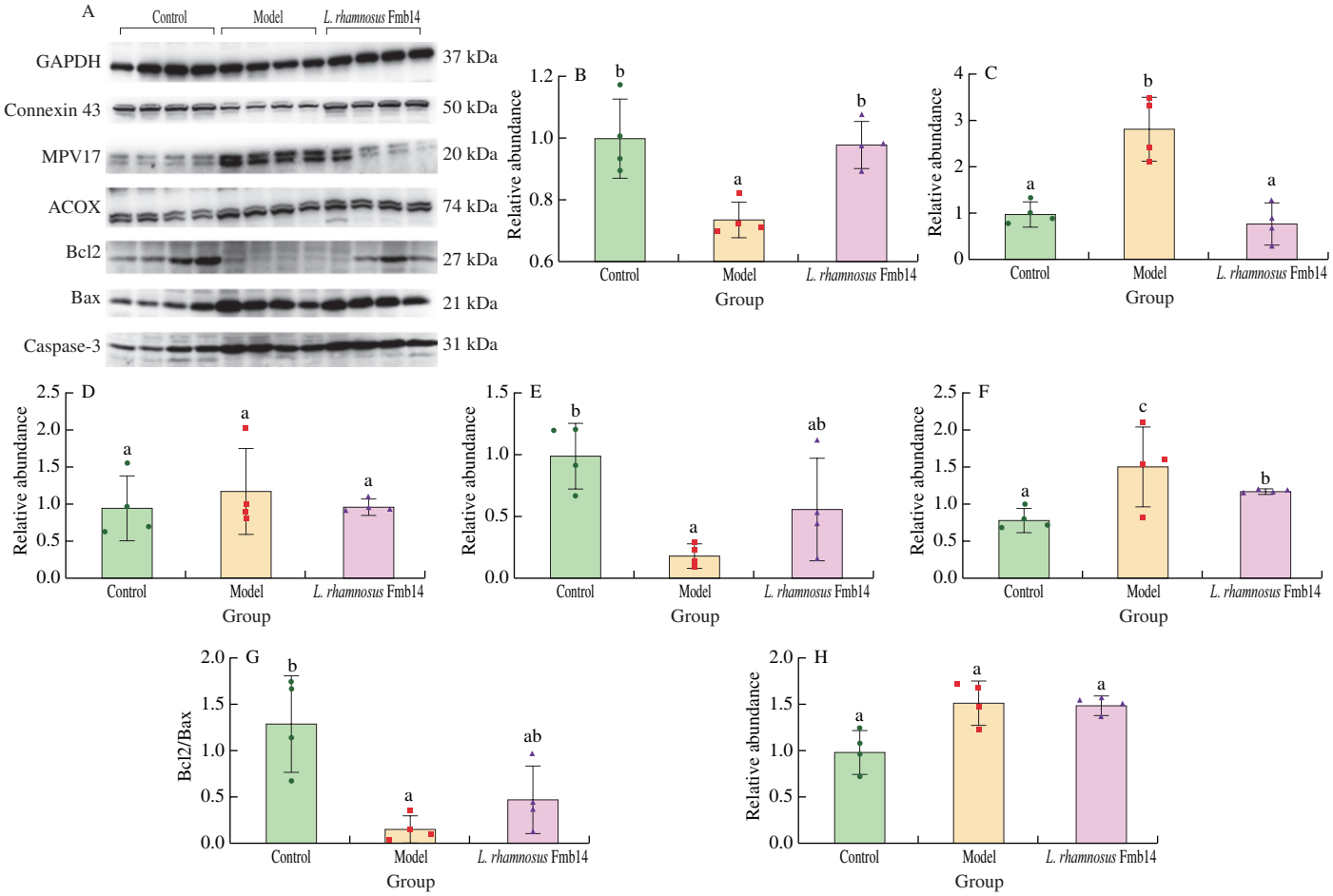

Fig. 6 *L. rhamnosus* Fmb14 administration improves mitochondrial injury and related apoptosis. (A) Western blot measurement of liver lysates from purine-induced hyperuricaemic mice without and with *L. rhamnosus* Fmb14 administration, including GAPDH, connexin 43, MPV17, Acox, Bcl2, Bax and caspase-3. Hepatic protein expression of (B) connexin 43, (C) MPV17, (D) Acox, (E) Bcl2, (F) Bax, (G) Bcl2/Bax, and (H) caspase-3. GAPDH was tested as a reference.

restored after *L. rhamnosus* Fmb14 administration (56% of control) (Figs. 6D, E and H), while the expression levels of Bax (1.52-fold of control) and caspase-3, the effectors of apoptosis, were both increased in the model group, and only Bax (1.18-fold of control) was ameliorated after *L. rhamnosus* Fmb14 administration (Fig. 6F). The Bcl2/Bax decreased from 1.31 (Control group) to 0.16 (Model group) when purine dietary conducted and increased to 0.48 (Fmb14 group) after *L. rhamnosus* Fmb14 administration (Fig. 6G). The Western blot results of Acox showed that the disorder of apoptosis at the mRNA level was not merely at the protein level.

The other abnormally elevated levels of p53 (1.70-fold of control), NF-κB (1.62-fold of control), AMPK (1.28-fold of control) and JNK (58% of control) indicated that pyroptosis was associated with a high risk of liver cancer. *L. rhamnosus* Fmb14 administration downregulated the risk factors in the livers of mice and the levels of p53 (1.04-fold of control), NF-κB (78% of control), AMPK (1.01-fold of control) and JNK (68% of control) (Figs. 7A-E). In addition, administration of *L. rhamnosus* Fmb14 exhibits no effect on the expression of AKT, CD36, ERK and Fas (Fig. S2).

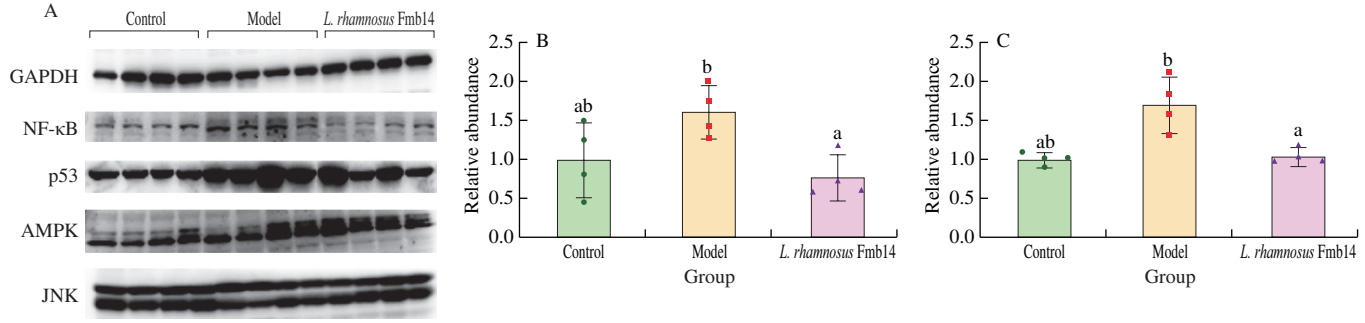

Fig. 7 *L. rhamnosus* Fmb14 administration decreased the tumour tendency of the liver. (A) Western blot measurement of liver lysates from purine-induced hyperuricaemic mice without and with *L. rhamnosus* Fmb14 administration, including GAPDH, NF-κB, p53, AMPK, and JNK. Hepatic protein expression of (B) NF-κB, (C) p53, (D) AMPK, and (E) JNK. GAPDH was tested as a reference.

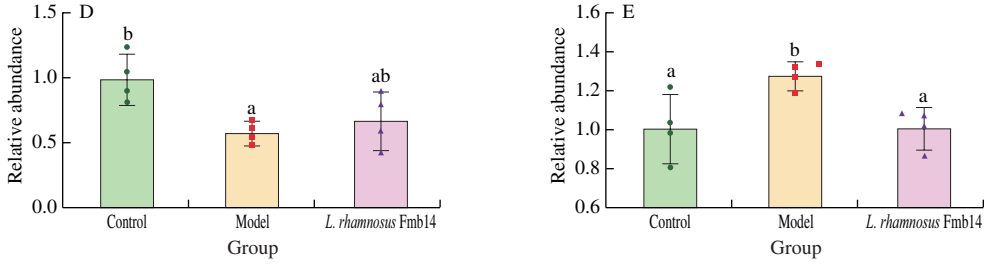

Fig. 7 (*Continued*)

4. Discussion

Hyperuricemia is widely accepted to increase the risk of gout and kidney injury, and therapeutic measures are often not recommended for people who remain asymptomatic condition[1]. High levels of UA in serum elevated the risk of gout, renal fibrosis and the inflammatory response[23], but few studies have focused on the damaging effects of UA on the liver. Studies of liver disease often focus on cirrhosis and steatohepatitis induced by alcohol or sugar[26], and the pathogenesis mechanisms of UA in the liver and probiotic preventive measures were discussed in this study. The results showed that abnormal death of hepatocytes increased when the levels of UA were increased to 500 μmol/L (Fig. 1A), which is consistent with the definition of hyperuricemia (480 μmol/L)[27]. Our previous research proved that the CFE of *L. rhamnosus* Fmb14 could modulate the metabolism of HepG2 cells in a high-purine environment[24], and treatment with CFE-H of *L. rhamnosus* Fmb14 also showed a positive effect on the modulation of death in HepG2 cells (Fig. 1). The same results were also proven in mice with dietary purine-induced hyperuricemia (Fig. 4). Our previous study proved that pretreatment with *L. rhamnosus* Fmb14 ameliorates dietary purine-induced hyperuricemia by restoring the gut microbiota structure and decreasing inflammatory levels in mice[23], and *L. rhamnosus* Fmb14 has a highly protective effect on hepatocyte injury by decreasing pyroptosis both *in vivo* and *in vitro*.

UA has been proven to aggravate myocardial failure and chronic kidney disease through the ROS and Nox4 signaling pathways, respectively[28-29]. The *L. rhamnosus* Fmb14 has been found to alleviate renal fibrosis in purine dietary hyperuricemia through gut-kidney axis and reduction of inflammatory response and oxidative stress were the main effect pathways that *L. rhamnosus* Fmb14 worked[24]. Systemic polyorganicity inflammation and oxidative stress was the characteristics of metabolic diseases like hyperuricemia and except for the kidney, liver is also attacked in the hyperuricemia based on our results. ROS is constantly produced and removed in the body accompanied by numerous metabolism reactions in the liver and the balance state of oxidative stress is important to drive regulatory signaling pathways. Metabolism disease such as hyperuricemia reduce the body's ability to consume oxygen free radicals[30] and excess ROS lead to intracellular proteins inactivation or degeneration, both of which could induce cell damage, and then multiple inflammatory response including NLRP3, NF-κB, tumor necrosis factor α (TNF-α), and nuclear factor-erythroid 2-related factor 2 (Nrf2) pathways were activated[31]. In addition, ROS and mitochondria play important roles in programmed cell death and mainly induce apoptosis initiated by signal transduction[32]. UA stimulation significantly increased all phases of the programmed death, while *L. rhamnosus* Fmb14 treatment mainly targeted the early phase (viable apoptotic cells) (Figs. 1B and C), which strongly indicated that *L. rhamnosus* Fmb14 treatment eliminated ROS and restored mitochondrial damage. Deficiency of autophagy or apoptosis causes ROS accumulation because a high level of DNA is released from damaged mitochondria[33]. ROS are among the signals that result in mitochondrial outer membrane permeabilization, which usually commits the cell to death[34]. The abnormal MMP caused by UA was restored by *L. rhamnosus* Fmb14 treatment (Fig. 2B). Pyroptosis is often caused by cytokines stimulated in cells and induces downstream reactions, such as inflammasome assembly or caspase-1 activation, which have been proven in many diseases[35]. As shown in Fig. 2A, ROS production was notably increased from 17.9% to 22.9% in the UA model group compared to the control group at 24 h ($P < 0.05$). Then, CFE-H treatment effectively reduced intracellular ROS to 14.5% in the UA model ($P < 0.05$) at 24 h. Cell death induced by different stimulations could clarify apoptosis, necroptosis, ferroptosis, pyroptosis and parthanatos[32], and the gene expression results revealed that *L. rhamnosus* Fmb14 treatment downregulated the pyroptosis induced by UA in HepG2 cells (Fig. 3A).

The perturbation of HepG2 homeostasis was triggered by UA[29,36] and the degree of pyroptosis was commonly linked with biomarkers such as NLRP3, caspase-1, IL-1β and IL-18[12]. The liver damage commonly considered as a synergistically effect by inflammation and oxidative stress and the degree of the liver injury often aggravated when the two pathway interacted in many metabolic disease such as type II diabetes or obesity[37]. The hyperuricemia induced liver damage was also consistent with the above hypothesis but the amelioration effect of *L. rhamnosus* Fmb14 on NLRP3 inflammasome cascade pathways proved inflammatory dominate the liver damage and oxidative stress was play an supporting role. NLRP3, a widely studied inflammasome that is involved in many damage signalling pathways and inflammatory reactions[12], has been verified to be activated to induce nonbacterial inflammation by many nonbiological danger signals, such as UA, ROS[29] and crystallization. As the sensor and effector of the NLRP3 inflammasome[19], the expression levels of NLRP3 and caspase-1 were found to be significantly decreased at both the mRNA and protein levels after *L. rhamnosus* Fmb14 treatment in UA-mediated HepG2 cell lines (Fig. 3). The recruitment of the NLRP3 inflammasome provides a molecular platform to enhance the secretion of cytokines, which act as distress signals to immune cells[12]. The major proinflammatory mediators released by NLRP3 inflammasome activation were IL-1β and IL-18, and the same decreasing trend of those two cytokines in the medium were found in the Fmb14-treated group compared to the UA model group (Figs. 3B and C). Here, we found a new *L. rhamnosus* Fmb14 that attenuated inflammation through NLRP3 inflammasome inhibition in UA-treated HepG2 cells.

Purine is metabolism precursor of UA which could mainly inducing hyperuricemia so that using purine-induced hyperuricemia as model to test protect effect of *L. rhamnosus* Fmb14 on hyperuricemia induced liver damage was more relevant to the reality than using UA directly and inosine has been proved no cytotoxicity to HepG2[24]. A high-purine diet causes UA metabolism disorders in the liver, and the redundant UA aggravates liver dysfunction in turn as a DAMP. Probiotics, especially *Lactobacillus* species, have been reported to modulate inflammation through inflammasome inhibition in PAMPs[38], but our results indicated that probiotic strategies also regulate the metabolism of the host to defend DAMPs. *L. rhamnosus* Fmb14 possess a superior colonization ability in the gut to benefit the host in purine diet induced hyperuricemia model[23]. To clarify the mechanisms by which *L. rhamnosus* Fmb14 alleviates UA-induced pyroptosis, the livers obtained from hyperuricemia mice induced by dietary purine were evaluated. Elevated serum UA has been reported to promote the process of nonalcoholic fatty liver disease[39] and hepatic steatosis[40] in mice. The livers of purine diet-induced hyperuricemia mice showed pathological changes through HE and TUNEL staining. *L. rhamnosus* Fmb14 administration eliminated the oedema and decreased the count of dead liver cells in hyperuricemia mice (Fig. 4), consistent with the views that beneficial microbes could regulate dietary disease through the gut-liver axis[41]. GSDMD and caspase-1 play roles as effectors and mediators in inflammatory pyroptosis[42] and the almost 6-fold increase in GSDMD in the model group compared to the control group explains the high rate of pyroptosis in the liver (Fig. 5). GSDMD exerts crucial functions in the processes of steatohepatitis[43] and cirrhosis[44], and we proved that hyperuricemia-related liver pyroptosis was another member of the NLRP3 pathway. In addition, pro-IL-1β was primed to activate IL-1β after the NLRP3 inflammasome was assembled by ASC, caspase-1 and NLRP3[12], and the inhibitory effect of *L. rhamnosus* Fmb14 on NLRP3 inflammasome cascade pathways revealed the ability of probiotics to regulate liver metabolism through the gut-liver axis[41].

Apoptosis and programmed cell death were commonly recognized as synonyms and pyroptosis was one type of abnormal cell death uniquely dependent on caspase-1[45]. Unregulated cell death progress underpins the sub-health state, and pyroptosis is one of the risk factors for tissues involved in tumorigenesis for the release of cytokines[46] and the GSDMD family[47]. The decrease of pyroptosis and increase of apoptosis in liver indicated that *L. rhamnosus* Fmb14 administration provide some kind of protective effect. Based on the results of low rate Bcl/Bax2, the apoptosis of hepatocyte was almost suppressed and the hepatocyte was dominated by the lytic and inflammatory type of programmed cell death. Additionally, mitochondrial outer membrane permeabilization induces cell death by proinflammatory signalling activation[34] and pyrimidine metabolism syndrome, leading to abnormal expression of MPV17[48]. MPV17 is a putative channel-forming protein of the inner mitochondrial membrane and it is involved in homeostasis of mitochondrial nucleotide metabolism. The levels of lactate and ROS were reported increased when *Mpv17* gene was knockdown in larvae through mitochondrial defects and our results implied high levels of UA resulted in abnormal expression of MPV17[49]. *L. rhamnosus* Fmb14 intervention reduced UA-induced pyroptosis by alleviating MMP abnormalities and eliminated cellular oedema to restore the expression of connexin 43, which provides a highly intact structure for hepatocytes[50]. Connexin 43 is a gap junction protein forming gap junctions and hemichannels in many tissues and it is reported that the expression of connexin 43 showed a high correlation with inflammation and its related cell death[51]. *L. rhamnosus* Fmb14 administration repaired the channels between hepatocytes to maintain metabolic homeostasis of ions or small-molecule exchange by upregulating the expression of connexin 43[52]. Fas, p53, and NF-κB have been classified as high-risk factors for inducing hepatocellular carcinoma when the cell death program is an irregular process[35], and these tumorigenesis biomarkers were found to be reduced after *L. rhamnosus* Fmb14 colonized hyperuricemia mice.

Lactobacillus is the most reported nonpathogenic endogenous bacterial genus and promotes the health of the host via gut microbiota regulation, immunological enhancement and metabolism modulation. The attenuation effects of *Lactobacillus* spp., including *Lactobacillus delbrueckii*, *Lactobacillus gasseri*, *L. reuteri* and *L. johnsonii*, on inflammation through NLRP3 inflammasome-dependent pathways have been researched, but all findings have shown that probiotics were efficient against immune response resistance mediated by pathogenic factors. The altered gut microbiota regulated by *L. rhamnosus* Fmb14 administration may contributes the ameliorated liver damage induced by hyperuricemia and *L. rhamnosus* Fmb14 administration altered the abundance of *Lactobacillus hamsteri*, *Lactobacillus vaginalis*, *Mucispirillum schaedleri*, *Butyricicoccus pullicaecorum*, *Parabacteroides distasonis*, [*Ruminococcus*] *gnavus*, and *Bacteroides acidifaciens* at species level[24]. Dietary-induced hyperuricemia promotes liver pyroptosis as a DAMP, and *L. rhamnosus* Fmb14 protects against liver damage by inhibiting the NLRP3 inflammasome, which is commonly recognized as a mechanism mediated by PAMPs. Although the evidence is strong, further research is also needed because factors of *in vivo* experiments have an interaction for dietary purine-altered gut microbiota and intestinal barriers to imbalance homeostasis, which could stimulate lymphocytes to release cytokines through the NLRP3 inflammasome.

The homeostasis of cells in the body maintains a steady rate of apoptosis, but high pyroptosis induced by hyperuricemia disrupts this balance. As the most important inhibitor of apoptosis, Bcl2 expression was found to be reduced to only 20% of the control, which means that the programmed death of cells tended to terminate. Bcl2 controls apoptosis, the mitochondrial suicide program, as a regulator of tumour development and tissue homeostasis[53]. As a response to inhibitor reduction, the two promoters of apoptosis, Bax and caspase-3, were upregulated in the hyperuricemia groups, and only Bax was recovered after *L. rhamnosus* Fmb14 administration (Fig. 6). Bax is one of the effectors in mitochondria that promotes apoptosis, and it is overexpressed when MOMP is altered in pyroptosis, which accelerates cell death[54]. The down-regulate trends of Bcl2/Bax indicated the normal programmed cell death has been inhibited while the total death rate of liver cells in model was higher than that in control group. High concentrations of serum UA lead to pyroptosis, and this uncontrolled cell death causes spillage of the contents of the cell into the blood circulation, which further stimulates inflammatory stress[55]. The internal environment is altered due to pyroptosis and failure of apoptosis, both of which result in forms of liver cancer[56]. Increased expression of the tumour suppressor p53 is associated with a high risk of cancer[34] and NF-κB signalling is also activated by pyroptosis to aggravate tissue damage[57]. p53 is not only considered a tumour suppressor but also participates in cellular metabolism, such

as oxidative phosphorylation, glycolysis and ROS[58]. In addition, *L. rhamnosus* Fmb14 administration also alleviated the stress response through JNK and AMPK pathway modulation, supporting the view that Bifidobacterium administration attenuates hepatic steatosis through the AMPK and JNK and NF-κB pathways[59].

In conclusion, the present study demonstrated that *L. rhamnosus* Fmb14 administration ameliorated pyroptosis induced by hyperuricemia in the HepG2 cell line and in mouse livers. Specifically, *L. rhamnosus* Fmb14 reduced pyroptosis in HepG2 cells through ROS reduction, MMP restoration and NLRP3 inflammasome inhibition. The amelioration effect of *L. rhamnosus* Fmb14 on pyroptosis was further proposed in purine-induced hyperuricemia mice, and the results indicated that *L. rhamnosus* Fmb14 administration reduced the total death rate of hepatocytes, and the protective effect contributed to the reduction in MPV17 and GSDMD and the enhancement of connexin 43. Moreover, *L. rhamnosus* Fmb14 also regulates disorders of apoptosis to attenuate the process of liver cancer. Therefore, *L. rhamnosus* Fmb14 mediates preventative effects on hyperuricemia-induced pyroptosis through NLRP3 inflammasome inhibition and MMP restoration.

Conflict of interest

We declare that we have no financial and personal relationships with other people or organizations that can inappropriately influence our work.

Acknowledgements

Grant support was received from the National Natural Science Foundation of China (32072182). We thank the College of Food Science and Technology, Nanjing Agricultural University for providing all necessary equipment.

Appendix A. Supplementary data

Supplementary data associated with this article can be found, in the online version, at http://doi.org/10.26599/FSHW.2022.9250181.

Reference

[1] L.A.B. Joosten, T.O. Crisan, P. Bjornstad, et al., Asymptomatic hyperuricaemia: a silent activator of the innate immune system, Nat. Rev. Rheumatol. 16 (2020) 75-86. https://doi.org/10.1038/s41584-019-0334-3.

[2] N. Dalbeth, H.K. Choi, L.A.B. Joosten, et al., Gout, Nat. Rev. Dis. Primers 5 (2019) 17.

[3] T. Jensen, M.F. Abdelmalek, S. Sullivan, et al., Fructose and sugar: a major mediator of non-alcoholic fatty liver disease, J. Hepatol. 68 (2018) 1063-1075. https://doi.org/10.1016/j.jhep.2018.01.019.

[4] R.J. Johnson, G.L. Bakris, C. Borghi, et al., Hyperuricemia, acute and chronic kidney disease, hypertension, and cardiovascular disease: report of a scientific workshop organized by the national kidney foundation, Am. J. Kidney Dis. 71 (2018) 851-865. https://doi.org/ 10.1053/j.ajkd.2017.12.009.

[5] T. Neogi, T.R. Mikuls, To treat or not to treat (to target) in gout, Ann. Intern. Med. 166 (2017) 71. https://doi.org/ https://doi.org/10.7326/M16-2401.

[6] J. Tian, B. Wang, B. Xie, et al., Pyroptosis inhibition alleviates potassium oxonate- and monosodium urate-induced gouty arthritis in mice, Mod. Rheumatol. 32 (2022) 221-230. https://doi.org/10.1080/14397595.2021.1899569.

[7] H.H. Chen, T.C. Yeh, P.W. Cheng, et al., Antihypertensive potential of coenzyme Q_{10} via free radical scavenging and enhanced Akt-nNOS signaling in the nucleus tractus solitarii in rats, Mol. Nutr. Food Res. 63 (2019) 1801042. https://doi.org/10.1002/mnfr.201801042.

[8] C. Kaneko, J. Ogura, S. Sasaki, et al., Fructose suppresses uric acid excretion to the intestinal lumen as a result of the induction of oxidative stress by NADPH oxidase activation, BBA-Gen. Subjects 1861 (2017) 559-566. https://doi.org/10.1016/j.bbagen.2016.11.042.

[9] Y. Wu, Z. Ye, P. Feng, et al., *Limosilactobacillus fermentum* JL-3 isolated from "Jiangshui" ameliorates hyperuricemia by degrading uric acid, Gut Microbes 13 (2021) 1-18. https://doi.org/10.1080/19490976.2021.1897211.

[10] K. Pavelcova, J. Bohata, M. Pavlikova, et al., Evaluation of the influence of genetic variants of SLC2A9 (GLUT9) and SLC22A12 (URAT1) on the development of hyperuricemia and gout, J. Clin. Med. 9 (2020) 17. https://doi.org/10.3390/jcm9082510.

[11] K.Y. Xu, S.R. Liu, X. Zhao, et al., Treating hyperuricemia related non-alcoholic fatty liver disease in rats with resveratrol, Biomed. Pharmacother. 110 (2019) 844-849. https://doi.org/10.1016/j.biopha.2018.12.039.

[12] M.S.J. Mangan, E.J. Olhava, W.R. Roush, et al., Targeting the NLRP3 inflammasome in inflammatory diseases, Nat. Rev. Drug Discov. 17 (2018) 588-606. https://doi.org/10.1038/nrd.2018.97.

[13] J. Tan, L. Wan, X. Chen, et al., Conjugated linoleic acid ameliorates high fructose-induced hyperuricemia and renal inflammation in rats via NLRP3 inflammasome and TLR4 signaling pathway, Mol. Nutr. Food Res. 63 (2019) 1801402. https://doi.org/10.1002/mnfr.201801402.

[14] R. Spiga, M.A. Marini, E. Mancuso, et al., Uric acid is associated with inflammatory biomarkers and induces inflammation via activating the NF-κB signaling pathway in HepG2 cells, Arterioscl. Throm. Vas. 37 (2017) 1241. https://doi.org/10.1161/ATVBAHA.117.309128.

[15] Y. Itahana, R. Han, S. Barbier, et al., The uric acid transporter SLC2A9 is a direct target gene of the tumor suppressor p53 contributing to antioxidant defense, Oncogene 34 (2015) 1799-1810. https://doi.org/10.1038/onc.2014.119.

[16] C.L. Gentile, T.L. Weir, The gut microbiota at the intersection of diet and human health, Science 362 (2018) 776-780. https://doi.org/10.1126/science.aau5812.

[17] Y. Wu, B. Wang, Z. Zeng, et al., Effects of probiotics *Lactobacillus plantarum* 16 and *Paenibacillus polymyxa* 10 on intestinal barrier function, antioxidative capacity, apoptosis, immune response, and biochemical parameters in broilers, Poultry Sci. 98 (2019) 5028-5039. https://doi.org/10.3382/ps/pez226.

[18] H. Zhao, Z. Lu, Y. Lu, The potential of probiotics in the amelioration of hyperuricemia, Food Funct. 13 (2022) 2394-2414. https://doi.org/10.1039/d1fo03206b.

[19] K.V. Swanson, M. Deng, J.P.Y. Ting, The NLRP3 inflammasome: molecular activation and regulation to therapeutics, Nat. Rev. Immunol. 19 (2019) 477-489. https://doi.org/10.1038/s41577-019-0165-0.

[20] Y. Yang, H.N. Wang, M. Kouadir, et al., Recent advances in the mechanisms of NLRP3 inflammasome activation and its inhibitors, Cell Death Dis. 10 (2019) 128. https://doi.org/10.1038/s41419-019-1413-8.

[21] V. Karaffova, V. Revajova, J. Koscova, et al., Local intestinal immune response including NLRP3 inflammasome in broiler chicken infected withCampylobacter jejuniafter administration of *Lactobacillus reuteri* B1/1, Food Agr. Immunol. 31 (2020) 937-949. https://doi.org/10.1080/09540105.2020.1788516.

[22] Y.J. Zou, J.J. Xu, X. Wang, et al., *Lactobacillus johnsonii* L531 ameliorates *Escherichia coli*-induced cell damage via inhibiting NLRP3 inflammasome activity and promoting ATG5/ATG16L1-mediated autophagy in porcine

mammary epithelial cells, Vet. Sci. 7 (2020) 112. https://doi.org/10.3390/vetsci7030112.

[23] H. Zhao, X. Chen, L. Zhang, et al., *Lacticaseibacillus rhamnosus* Fmb14 prevents purine induced hyperuricemia and alleviate renal fibrosis through gut-kidney axis, Pharmacol. Res. 182 (2022) 106350. https://doi.org/10.1016/j.phrs.2022.106350.

[24] H. Zhao, X. Chen, F. Meng, et al., Ameliorative effect of *Lacticaseibacillus rhamnosus* Fmb14 from Chinese yogurt on hyperuricemia, Food Sci. Hum. Wellness 12 (2023) 1379-1390. https://doi.org/10.1016/j.fshw.2022.10.031.

[25] L.L. Liu, R. Jin, J.Q. Hao, et al., Consumption of the fish oil high-fat diet uncouples obesity and mammary tumor growth through induction of reactive oxygen species in protumor macrophages, Cancer Res. 80 (2020) 2564-2574. https://doi.org/10.1158/0008-5472.CAN-19-3184.

[26] V.W.S. Wong, S. Chitturi, G.L.H. Wong, et al., Pathogenesis and novel treatment options for non-alcoholic steatohepatitis, Lancet Gastroenterol. 1 (2016) 56-67. https://doi.org/10.1016/S2468-1253(16)30011-5.

[27] R. Terkeltaub, Update on gout: new therapeutic strategies and options, Nat. Rev. Rheumatol. 6 (2010) 30-38. https://doi.org/10.1038/nrrheum.2009.236.

[28] Z. Li, Y. Sheng, C. Liu, et al., Nox4 has a crucial role in uric acid-induced oxidative stress and apoptosis in renal tubular cells, Mol. Med. Rep. 13 (2016) 4343-4348. https://doi.org/10.3892/mmr.2016.5083.

[29] S. Shen, F. He, C. Cheng, et al., Uric acid aggravates myocardial ischemia-reperfusion injury via ROS/NLRP3 pyroptosis pathway, Biomed. Pharm. 133 (2021) 110990. https://doi.org/10.1016/j.biopha.2020.110990.

[30] Y.Z. Zhang, Y.Q. Li, X.X. Ren, et al., The positive correlation of antioxidant activity and prebiotic effect about oat phenolic compounds, Food Chem. 402 (2023) 134231. https://doi.org/10.1016/j.foodchem.2022.134231.

[31] Z. Xian, Y.H. Choi, M. Zheng, et al., Imperatorin alleviates ROS-mediated airway remodeling by targeting the Nrf2/HO-1 signaling pathway, Biosci. Biotech. Bioch. 84 (2020) 898-910. https://doi.org/10.1080/09168451.2019.1710107.

[32] L. Galluzzi, I. Vitale, S.A. Aaronson, et al., Molecular mechanisms of cell death: recommendations of the Nomenclature Committee on Cell Death 2018, Cell Death Differ. 25 (2018) 486-541. https://doi.org/10.1038/s41418-017-0012-4.

[33] Z.Y. Zhong, A. Umemura, E. Sanchez-Lopez, et al., NF-κB restricts inflammasome activation via elimination of damaged mitochondria, Cell 164 (2016) 896-910. https://doi.org/10.1038/s41418-017-0012-4.

[34] F.J. Bock, S.W.G. Tait, Mitochondria as multifaceted regulators of cell death, Nat. Rev. Mol. Cell Bio. 21 (2020) 85-100. https://doi.org/10.1038/s41580-019-0173-8.

[35] Y.L. Hsu, P.L. Kuo, L.C. Chiang, et al., Involvement of p53, nuclear factor kappa B and Fas/Fas ligand in induction of apoptosis and cell cycle arrest by saikosaponin d in human hepatoma cell lines, Cancer Lett. 213 (2004) 213-221. https://doi.org/10.1016/j.canlet.2004.03.044.

[36] I. Jorgensen, E.A. Miao, Pyroptotic cell death defends against intracellular pathogens, Immunol. Rev. 265 (2015) 130-142. https://doi.org/10.1111/imr.12287.

[37] Y. Li, C. Qin, L.Z. Dong, et al., Whole grain benefit: synergistic effect of oat phenolic compounds and beta-glucan on hyperlipidemia via gut microbiota in high-fat-diet mice, Food Funct. 13 (2022) 12686-12696. https://doi.org/10.1039/d2fo01746f.

[38] M. Miettinen, T.E. Pietila, R.A. Kekkonen, et al., Nonpathogenic *Lactobacillus rhamnosus* activates the inflammasome and antiviral responses in human macrophages, Gut Microbes 3 (2012) 510-522. https://doi.org/10.4161/gmic.21736.

[39] Y.J. Choi, H.S. Shin, H.S. Choi, et al., Uric acid induces fat accumulation via generation of endoplasmic reticulum stress and SREBP-1c activation in hepatocytes, Lab. Invest. 94 (2014) 1114-1125. https://doi.org/10.1038/labinvest.2014.98.

[40] X.Y. Wan, C.F. Xu, Y.M. Lin, et al., Uric acid regulates hepatic steatosis and insulin resistance through the NLRP3 inflammasome-dependent mechanism, J. Hepatol. 64 (2016) 925-932. https://doi.org/10.1016/j.jhep.2015.11.022.

[41] A. Albillos, A. de Gottardi, M. Rescigno, The gut-liver axis in liver disease: pathophysiological basis for therapy, J. Hepatol. 72 (2020) 558-577. https://doi.org/10.1016/j.jhep.2019.10.003.

[42] J. Shi, Y. Zhao, K. Wang, et al., Cleavage of GSDMD by inflammatory caspases determines pyroptotic cell death, Nature 526 (2015) 660-665. https://doi.org/10.1038/nature15514.

[43] B. Xu, M.Z. Jiang, Y. Chu, et al., Gasdermin D plays a key role as a pyroptosis executor of non-alcoholic steatohepatitis in humans and mice, J. Hepatol. 68 (2018) 773-782. https://doi.org/10.1016/j.jhep.2017.11.040.

[44] S. Das, M. Miller, D.H. Broide, Chromosome 17q21 genes *ORMDL3* and *GSDMB* in asthma and immune diseases, in: F.W. Alt (Eds.), *Advances in Immunology*, 2017, pp. 1-52. https://doi.org/10.1016/bs.ai.2017.06.001.

[45] S.L. Fink, B.T. Cookson, Apoptosis, pyroptosis, and necrosis: mechanistic description of dead and dying eukaryotic cells, Infect. Immun. 73 (2005) 1907-1916. https://doi.org/10.1128/IAI.73.4.1907-1916.2005.

[46] X.J. Xia, X. Wang, Z. Cheng, et al., The role of pyroptosis in cancer: pro-cancer or pro-"host"?, Cell Death Dis. 10 (2019) 650. https://doi.org/10.1038/s41419-019-1883-8.

[47] J. Ding, K. Wang, W. Liu, et al., Pore-forming activity and structural autoinhibition of the gasdermin family, Nature 535 (2016) 111-116. https://doi.org/ 10.1038/nature18590.

[48] J.R. Alonzo, C. Venkataraman, M.S. Field, et al., The mitochondrial inner membrane protein MPV17 prevents uracil accumulation in mitochondrial DNA, J. Bio. Chem. 293 (2018) 20285-20294. https://doi.org/10.1074/jbc.RA118.004788.

[49] A. Kodani, M. Yamaguchi, R. Itoh, et al., A *Drosophila* model of the neurological symptoms in Mpv17-related diseases, Sci. Rep. 12 (2022) 22632. https://doi.org/10.1038/s41598-022-27329-x.

[50] R.S. Tonkin, C. Bowles, C.J. Perera, et al., Attenuation of mechanical pain hypersensitivity by treatment with Peptide5, a connexin-43 mimetic peptide, involves inhibition of NLRP3 inflammasome in nerve-injured mice, Exp. Neurol. 300 (2018) 1-12. https://doi.org/10.1016/j.expneurol.2017.10.016.

[51] M. Dosch, J. Zindel, F. Jebbawi, et al., Connexin-43-dependent ATP release mediates macrophage activation during sepsis, eLife 8 (2019) e42670. https://doi.org/10.7554/eLife.42670.

[52] R.S. Tonkin, Y. Mao, S.J. O'Carroll, et al., Gap junction proteins and their role in spinal cord injury, Front. Mol. Neurosci. 7 (2014) 102. https://doi.org/10.3389/fnmol.2014.00102.

[53] F. Edlich, BCL-2 proteins and apoptosis: recent insights and unknowns, Biochem. Bioph. Res. Co. 500 (2018) 26-34. https://doi.org/10.1016/j.bbrc.2017.06.190.

[54] L. Lartigue, Y. Kushnareva, Y. Seong, et al., Caspase-independent mitochondrial cell death results from loss of respiration, not cytotoxic protein release, Mol. Biol. Cell 20 (2009) 4871-4884. https://doi.org/10.1091/mbc.e09-07-0649.

[55] M.S. D'Arcy, Cell death: a review of the major forms of apoptosis, necrosis and autophagy, Cell Bio. Int. 43 (2019) 582-592. https://doi.org/10.1002/cbin.11137.

[56] M. Seehawer, F. Heinzmann, L. D'Artista, et al., Necroptosis microenvironment directs lineage commitment in liver cancer, Nature 562 (2018) 69. https://doi.org/10.1038/s41586-018-0519-y.

[57] F.G. Bauernfeind, G. Horvath, A. Stutz, et al., Cutting edge: NF-κB activating pattern recognition and cytokine receptors license NLRP3 inflammasome activation by regulating NLRP3 expression, J. Immunol. 183 (2009) 787-791. https://doi.org/10.4049/jimmunol.0901363.

[58] E.M. Kim, C.H. Jung, J. Kim, et al., The p53/p21 complex regulates cancer cell invasion and apoptosis by targeting Bcl-2 family proteins, Cancer Res. 77 (2017) 3092-3100. https://doi.org/10.1158/0008-5472.CAN-16-2098.

[59] Y. Yan, C.Y. Liu, S.M. Zhao, et al., Probiotic *Bifidobacterium lactis* V9 attenuates hepatic steatosis and inflammation in rats with non-alcoholic fatty liver disease, AMB Express 10 (2020) 1-11. https://doi.org/10.1186/s13568-020-01038-y.